Deletion of calcineurin from astrocytes reproduces proteome signature of Alzheimer's disease and epilepsy and predisposes to seizures.

Laura Tapella[a1], Giulia Dematteis[a1], Federico Alessandro Ruffinatti[a], Luisa Ponzoni[b], Fabio Fiordaliso[c], Alessandro Corbelli[c], Enrico Albanese[a], Beatrice Pistolato[a], Jessica Pagano[d], Elettra Barberis[e,f], Emilio Marengo[e] Claudia Balducci[g], Gianluigi Forloni[g], Chiara Verpelli[d], Carlo Sala[d], Carla Distasi[a], Mariaelvina Sala[d], Armando A Genazzani[a], Marcello Manfredf[f,h,2], Dmitry Lim[a,2,3].

[a] Department of Pharmaceutical Sciences, Università del Piemonte Orientale "Amedeo Avogadro", Via Bovio 6, 28100, Novara, Italy;
[b] BIOMETRA, University of Milan and Fondazione Zardi-Gori, Milan, Italy
[c] Department of Cardiovascular Research, Istituto di Ricerche Farmacologiche Mario Negri IRCCS, Milan, Italy.
[d] CNR Neuroscience Institute, Milan, Italy
[e] Department of Sciences and Technological Innovation, Università del Piemonte Orientale, Alessandria, Italy.
[f] Department of Translational Medicine, University of Piemonte Orientale, Novara, Italy.
[g] Department of Neuroscience, Istituto di Ricerche Farmacologiche Mario Negri IRCCS, Milan, Italy.
[h] Center for Translational Research on Autoimmune and Allergic Diseases, University of Piemonte Orientale, Novara, Italy.

[1] These Authors contributed equally.

[2] These Authors share seniorship.

[3] Correspondence should be sent to: Dmitry Lim, dmitry.lim@uniupo.it, Tel.: +39-0321 375822

ABSTRACT

Calcineurin (CaN), acting downstream of intracellular calcium signals, orchestrates cellular remodelling in many cellular types. In astrocytes, principal homeostatic cells in the central nervous system (CNS), CaN is involved in neuroinflammation and gliosis, while its role in healthy CNS or in early neuro-pathogenesis is poorly understood. Here we report that in mice with conditional deletion of CaN from GFAP-expressing astrocytes (astroglial calcineurin KO, ACN-KO), at 1 month of age, transcription was not changed, while proteome was deranged in hippocampus and cerebellum. Gene ontology analysis revealed overrepresentation of annotations related to myelin sheath, mitochondria, ribosome and cytoskeleton. Overrepresented pathways were related to protein synthesis, oxidative phosphorylation, mTOR and neurological disorders, including Alzheimer's disease (AD) and seizure disorder. Comparison with published proteomics datasets shows significant overlap with the proteome of a familial AD mouse model and of human subjects with drug-resistant epilepsy. Strikingly, beginning from about 5 months of age ACN-KO mice develop spontaneous tonic-clonic seizures with inflammatory signature of epileptic brain. Altogether, our data suggest that the deletion of astroglial CaN produces features of neurological disorders and predisposes mice to seizures. We suggest that calcineurin in astrocytes may serve as a novel Ca^{2+}-sensitive switch which regulates protein expression and homeostasis in the central nervous system.

INTRODUCTION

Homeostatic support, provided by astrocytes, is of paramount importance for correct neuronal function (Verkhratsky and Nedergaard, 2018). During continuous interaction with cells in the CNS, astrocytes generate intracellular calcium (Ca^{2+}) signals which are thought to mediate their homeostatic activities, including release of signalling molecules, control of cerebral blood flow, regulation of K^+ and neurotransmitter uptake and control of neuronal activity (Khakh and Sofroniew, 2015). Moreover, deregulation of astrocytic Ca^{2+} signals and downstream signalling processes are strongly associated with neuropathologies including Alzheimer's disease and epilepsy (Lim et al., 2016b; Nikolic et al., 2019). Much effort has been dedicated to detection and characterization of astroglial Ca^{2+} signals themselves (Fiacco et al., 2009; Bindocci et al., 2017), while how the Ca^{2+} signals in astrocytes are decoded, processed and translated to arrange a multitude of astroglial homeostatic activities is poorly understood.

Recently, we have generated a mouse with conditional KO of calcineurin (CaN), a Ca^{2+}/calmodulin-activated serine-threonine phosphatase (astroglial calcineurin KO, or ACN-KO) and showed that the deletion of astrocytic CaN (Astro-CaN) severely impairs intrinsic neuronal excitability through functional inactivation of astroglial Na^+/K^+ ATPase and deregulation of Na^+ and K^+ handling (Tapella et al., 2020). CaN drives Ca^{2+}-dependent cellular transcriptional and functional remodelling in different cellular types including lymphocytes (Oh-hora and Rao, 2008), cardiomyocytes (Parra and Rothermel, 2017), skeletal muscle (Tu et al., 2016), bone cells (Sitara and Aliprantis, 2010) and neurons (Baumgärtel and Mansuy, 2012). However it is not known whether in healthy astrocytes CaN exerts similar activity and the targets of the activity-dependent CaN activation (Lim et al., 2018) are not known.

In the present report we used multiomics approach to comprehensively investigate alterations produced by the deletion of Astro-CaN at transcriptional and proteome levels. We report that the deletion of CaN from astrocytes, at one month of age, results in derangement of protein expression at the posttranscriptional level re-creating protein profile associated with neurological and neurodegenerative diseases, in particular with AD and seizures. Later in life, beginning from about 5 months of age, ACN-KO mice demonstrate increasing risk to develop spontaneous tonic-clonic motor seizures. Collectively, our results suggest that Astro-CaN may serve as a Ca^{2+}-sensitive molecular hub which regulates protein expression and homeostasis in the CNS.

METHODS

Generation and handling of ACN-KO mice

Generation and handling of conditional CaN knockout (KO) in GFAP-expressing astrocytes (astroglial calcineurin KO, ACN-KO) has been described previously (Tapella et al., 2020). Briefly, CaNB1$^{flox/flox}$ mice (Neilson et al., 2004) (Jackson Laboratory strain B6;129S-Ppp3r1tm2Grc/J, stock number 017692) has been with crossed with GFAP-Cre mice (Gregorian et al., 2009) (Jackson Laboratory strain B6.Cg-Tg(Gfap-cre)77.6Mvs/2J, stock number 024098). The line was maintained by crossing CaNB1$^{flox/flox}$/GfapCre$^{-/-}$ (thereafter referred as to ACN-Ctr) males with CaNB1$^{flox/flox}$/GfapCre$^{+/-}$ (ACN-KO) females.

Mice were housed in the animal facility of the Università del Piemonte Orientale, with unlimited access to water and food. Animals were managed in accordance with European directive 2010/63/UE and with Italian law D.l. 26/2014. The procedures were approved by the local animal-health and ethical committee (Università del Piemonte Orientale) and were authorized by the national authority (Istituto Superiore di Sanità; authorization numbers N. 77-2017 and N. 214-2019). All efforts were made to reduce the number of animals by following the 3R's rule.

Next Generation RNA sequencing (RNA-Seq)

For RNA-Seq, total RNA from hippocampal and cerebellar tissues were extracted using SPLIT RNA Extraction Kit (Cat. 00848; Lexogen GmbH, Vienna, Austria) according to manufacturer's instructions. 200 ng of RNA were subjected to an Illumina sequencing using Lexogen QuantSeq FWD - SR75 - DA Service. Reads were mapped to the reference genome using STAR aligner v2.7 (Dobin et al., 2013), while the differential expression analysis was performed with DESeq2 v1.26 Bioconductor package (Love et al., 2014) (Love et al. 2014). Six (6) animals per condition were independently processed from 1 month old ACN-Ctr and ACN-KO mice.

Isolation of total RNA and real-time PCR

For validation of RNA-Seq and shotgun proteomics results samples were prepared from a separate set of 12 ACN-Ctr and ACN-KO 1 month old mice.

For real-time PCR, hippocampal or cerebellar tissues from one animal were lysed in Trizol reagent (Invitrogen, Cat. 15596026). Total RNA was extracted using according to manufacturer's instructions using chloroform extraction followed by isopropanol precipitation. After washing with 75% ethanol, RNA was dried and resuspended in 20-30 µL of RNAse-free water. 0.5-1 µg of total RNA was retrotranscribed using SensiFAST cDNA Synthesis Kit (BioLine, London, UK). Real-time PCR was performed using iTaq qPCR master mix according to manufacturer's instructions (Bio-Rad, Segrate, Italy, Cat. 1725124) on a SFX96 Real-time system (Bio-Rad). To normalize raw real-time PCR data, S18 ribosomal subunit was used. Sequences of oligonucleotide primers is listed in SI Appendix Methods Table 1. The real-time PCR data are expressed as delta-C(t) of gene of interest to S18 allowing appreciation of the expression level of a single gene.

Preparations of tissue homogenates and synaptosomal fractions

Tissues were homogenized using glass-Teflon 1 ml homogenizer, lysed (lysis buffer: 50 mM Tris HCl (pH 7.4), sodium dodecyl sulfate (SDS) 0.5%, 5 mM EDTA). Synaptosomal fractions were

prepared as reported previously (Gillardon, 2006) from hippocampal or cerebellar tissues pooled from two 1 month old ACN-Ctr or ACN-KO mice. Briefly, mice were anesthetized by intraperitoneal injection of Zoletil (80 mg/kg) and Xylazine (45 mg/kg) and sacrificed by decapitation. Hippocampal formations and cerebella were rapidly dissected and placed into ice-cold homogenization buffer containing 50 mM MOPS, pH 7.4, 320 mM sucrose, 0.2 mM DTT, 100 mM KCl, 0.5 mM $MgCl_2$, 0.01 mM EDTA, 1 mM EGTA, protease inhibitor cocktails (PIC, Calbiochem) and phosphatase inhibitor Na_3VO_4 (1µM). All subsequent steps were performed at 4°C. The tissues were minced and homogenized in 1:10 w/v homogenization buffer with 12 strokes in a Teflon-glass douncer. The homogenates centrifuged for 10 min at 800 xg followed by centrifugation of the supernatant at 9200 xg for 15 min. The resulting P2 pellet, representing the crude synaptosomal fraction, was solubilized in lysis buffer.

Western blot

20 µg proteins were resolved on 8% of 12% SDS-polyacrylamide gel. Proteins were transferred onto nitrocellulose membrane using Trans-Blot Turbo Transfer System (Bio-Rad), blocked in skim milk (5%, for 1 h; Cat. 70166; Sigma) and immunoblotted with indicated antibody. Mouse anti-Tubulin (1:5000, Cat. T7451) or anti-β-actin (1:10000, Cat. A1978), both from Sigma (https://www.sigmaaldrich.com/) were used to normalize protein load. Primary antibodies were: mouse anti-Sy38 (1:500, Cat. MAB-10321); rabbit anty-Cox6a1 (1:500, Cat. AB-83898); rabbit anti-Vdac2 (1:500, Cat. AB-83899); rabbit anti-Atp5j (1:500, Cat. AB-83897); rabbit anti-Dpysl4 (1:500, Cat. AB-83901); rabbit anti-Gfap (1:500, Cat. N. AB-10682), all from Immunological Sciences (http://www.immunologicalsciences.com/home); rabbit anty-Rps10 (1:500, Cat. PA5-96460, Thermofisher, https://www.thermofisher.com/); rabbit anty-Glast (1:500, Cat. NB100-1869, NovusBio, https://www.novusbio.com/); rabbit anty-Atp1a2 (1:1000, Cat. ANP-002, Alomone Labs, https://www.alomone.com/); mouse anti-PSD95, clone K28/43 (1 : 1000, Cat. MABN68, Merck Millipore, https://www.merckmillipore.com/); mouse anti-Snap25 (1:600, Cat. sc-376713, SantaCruz, https://www.scbt.com/home). Goat anti-mouse IgG (H+L) horseradish peroxidase-conjugated secondary antibody (1 : 8000; Cat. 170-6516, Bio-Rad, https://www.bio-rad.com/) was used. The protein bands were developed using SuperSignal West Pico chemiluminescent substrate (Cat. 34078; Thermofisher). Densitometry analysis was performed using Quantity One software (Bio-Rad).

Proteomic analysis

In solution digestion

Lysates were digested using the following protocol: samples were prepared to have 100 µg of protein in a final volume of 25 µL of 100 mM NH_4HCO_3. Proteins were reduced using 2.5 µL of dithiothreitol (200 mM DTT stock solution) (Sigma) at 90 °C for 20 min, and alkylated with 10 µl of Cysteine Blocking Reagent (Iodoacetamide, IAM, 200 mM Sigma) for 1 h at room temperature in the dark. DTT stock solution was then added to destroy the excess of IAM. After dilution with 300 µL of water and 100 µL of NH_4HCO_3 to raise pH 7.5-8.0, 5 µg of trypsin (Promega, Sequence Grade) was added and digestion was performed overnight at 37 °C. Trypsin activity was stopped by adding 2 µL of neat formic acid and samples were dried by Speed Vacuum (Rocchio et al., 2019).

The peptide digests were desalted on the Discovery® DSC-18 solid phase extraction (SPE) 96-well Plate (25 mg/well) (Sigma-Aldrich Inc., St. Louis, MO, USA). The SPE plate was preconditioned with 1 mL of acetonitrile and 2 mL of water. After the sample loading, the SPE was washed with 1

mL of water. The adsorbed proteins were eluted with 800 µL of acetonitrile:water (80:20). After desalting, samples were vacuum evaporated and reconstituted with 20 µL of 0.05% formic acid in water. Two µL of stable-isotope-labeled peptide standard (DPEVRPTSAVAA, Val- 13C5 15N1 at V10, Cellmano Biotech Limited, Anhui, China) was spiked into the samples before the LC-MS/MS analysis and used for instrument quality control.

Label-free proteomic analysis

LC–MS/MS analyses were performed using a micro-LC Eksigent Technologies (Dublin, USA) system with a stationary phase of a Halo Fused C18 column (0.5 × 100 mm, 2.7 µm; Eksigent Technologies, Dublin, USA). The injection volume was 4.0 µL and the oven temperature was set at 40 °C. The mobile phase was a mixture of 0.1% (v/v) formic acid in water (A) and 0.1% (v/v) formic acid in acetonitrile (B), eluting at a flow-rate of 15.0 µL min^{-1} at an increasing concentration of solvent B from 2% to 40% in 30 min. The LC system was interfaced with a 5600+ TripleTOF system (AB Sciex, Concord, Canada) equipped with a DuoSpray Ion Source and CDS (Calibrant Delivery System). Samples used to generate the SWATH-MS (Sequential window acquisition of all theoretical mass spectra) spectral library were subjected to the traditional data-dependent acquisition (DDA): the mass spectrometer analysis was performed using a mass range of 100–1500 Da (TOF scan with an accumulation time of 0.25 s), followed by a MS/MS product ion scan from 200 to 1250 Da (accumulation time of 5.0 ms) with the abundance threshold set at 30 cps (35 candidate ions can be monitored during every cycle). Samples were then subjected to cyclic data independent analysis (DIA) of the mass spectra, using a 25-Da window. A 50-ms survey scan (TOF-MS) was performed, followed by MS/MS experiments on all precursors. These MS/MS experiments were performed in a cyclic manner using an accumulation time of 40 ms per 25-Da swath (36 swaths in total) for a total cycle time of 1.5408 s. The ions were fragmented for each MS/MS experiment in the collision cell using the rolling collision energy. The MS data were acquired with Analyst TF 1.7 (SCIEX, Concord, Canada). Three instrumental replicates for each sample were subjected to the DIA analysis (Martinotti et al., 2016; Dalla Pozza et al., 2018).

Protein Database Search

The mass spectrometry files were searched using Protein Pilot (AB SCIEX, Concord, Canada) and Mascot (Matrix Science Inc., Boston, USA). Samples were input in the Protein Pilot software v4.2 (AB SCIEX, Concord, Canada), which employs the Paragon algorithm, with the following parameters: cysteine alkylation, digestion by trypsin, no special factors and False Discovery Rate at 1%. The UniProt Swiss-Prot reviewed database containing mouse proteins (version 12/10/2018, containing 25137 sequence entries). The Mascot search was performed on Mascot v2.4, the digestion enzyme selected was trypsin, with 2 missed cleavages and a search tolerance of 50 ppm was specified for the peptide mass tolerance, and 0.1 Da for the MS/MS tolerance. The charges of the peptides to search for were set to 2 +, 3 + and 4 +, and the search was set on monoisotopic mass. The instrument was set to ESI-QUAD-TOF and the following modifications were specified for the search: carbamidomethyl cysteines as fixed modification and oxidized methionine as variable modification.

Protein quantification

The quantification was performed by integrating the extracted ion chromatogram of all the unique ions for a given peptide. The quantification was carried out with PeakView 2.0 and MarkerView 1.2. (Sciex, Concord, ON, Canada). Six peptides per protein and six transitions per peptide were extracted from the SWATH files. Shared peptides were excluded as well as peptides with modifications. Peptides with FDR lower than 1.0% were exported in MarkerView for the t-test.

Cell specificity analysis

To assess cell specificity, two databased were primed: Human Protein Atlas (HPA, https://www.proteinatlas.org/) and the mouse brain cells-specific RNA-Seq database contributed by (Zhang et al., 2014). HPA immunoreactivity scores in glial cells and neurons were labelled as: NA (not assayed), ND (not detected, score = 0), Low (score = 1), Medium (score = 3) and High (score = 4). Hits with a score = 0 in glial cells and score > 0 in neurons was assigned to as Neuron-specific; hits in which score ≠ 0 and neuron (N)/glia (G) ratio > 1 were assigned to as Enriched in neurons; hits in which score ≠ 0 and N/G ratio = 1 were assigned to as Ubiquitous; hits in which score ≠ 0 and N/G ratio < 1 were assigned to as Enriched in glia; and hits with a score = 0 in neurons and score > 0 in glia were assigned to as Glia-specific.

To score Zhang et al database, excel files with Mean FPKM cell-specific values were downloaded. For each gene, ratios were calculated as (Neurons)/(All other cell types); (Astrocytes)/(All other cell types); (Oligodendrocyte Precursor Cells + Non-myelinating Oligodendrocytes + Myelinating Oligodendrocytes)/(All other cell types); (Microglia)/(All other cells types). Genes with ratios > 5 were assigned as cell-type specific, and the presence of these genes in HIP ACN-KO list was specified.

Bioinformatics analysis

For bioinformatics analysis, DEPs from whole tissue preparations were pooled with correspondent synaptosomal DEPs: Wht-Hip ∪ Syn-Hip = HIP; Wht-Cb ∪ Syn-Cb = CB. Wht-Hip and Syn-Hip did not contain common DEPs at |FC| > 1.5 and p-value < 0.05 and were pooled without modifications. Wht-Cb and Syn-Cb (|FC| > 1.5 and p-value < 0.05) contained 3 common DEPs. In this case the DEP with lower p-value regardless of its FC was taken for further analysis. This resulted 155 and 54 unique DEPs in HIP and CB lists, respectively.

DAVID gene ontology (GO) analysis.

Gene ontology (GO) analysis was performed using The Database for Annotation, Visualization and Integrated Discovery (DAVID) v.6.8 tool (https://david.ncifcrf.gov/) (Huang et al., 2009). Overrepresented GO terms which passed Benjamini correction ($p < 0.05$) were considered significant.

STRING protein-protein interaction analysis.

For prediction of protein-protein interactions and clustering using K-means algorithm, Search Tool for the Retrieval of Interacting Genes/Proteins (STRING) v10.5 online software was used (https://string-db.org/) (Szklarczyk et al., 2017).

IPA pathway analysis

For pathway analysis, Ingenuity Pathway Analysis package (Content version: 49932394; Release Date: 2019-11-14) was used. Ingenuity Canonical Pathways, Disease and Bio Functions, Upstream Regulators and Causal Network Regulators were downloaded using default settings.

Comparison with AD and epilepsy datasets

HIP ACN-KO differential protein expression was compared with published mouse AD and human epilepsy proteome datasets. The proteomics analysis by Neuner et al. (2017) on 8-month-old 5xFAD hippocampus mouse model was used as AD reference and DEPs were matched by primary accession number as retrieved from the UniProtKB/Swiss-Prot reviewed database (release 2020_01). The dataset provided by Keren-Aviram et al. (2018) on human refractory epilepsy was used as epileptic

reference. In this case, to allow interspecies comparison, BioMart tool (www.ensembl.org) was used to extract genes that were orthologous between human and mouse. Afterwards, DEPs were again matched by primary accession number. In both the cases, the significance of the overlap between sets was evaluated through hypergeometric test, using as background reference the number of protein-coding transcripts detected by RNA-Seq (N=14,333 genes).

Transmission electron microscopy

ACN-Ctr and ACN-KO mice were deeply anesthetized and perfused through the ascending aorta with phosphate buffered saline (PBS, 0.1 M; pH 7.4) and heparin (1.25 unit/ml) for not more than 2 minutes, followed by a 20 minute perfusion with 2% paraformaldehyde (PFA) and 2.5% glutaraldehyde in PBS. Hippocampus was excised and cut in sagittal plane with a razor blade and postfixed in 4% paraformaldehyde (PFA) and 2% glutaraldehyde in PBS and then for 2 h in OsO_4. After dehydration in graded series of ethanol, tissue samples were cleared in propylene oxide, embedded in Epoxy medium (Epon 812 Fluka) and polymerized at 60 °C for 72 h. From each sample, one semithin (1 μm) section was cut with a Leica EM UC6 ultramicrotome and mounted on glass slides for light microscopic inspection. Ultrathin (70 nm thick) sections of areas of interest were obtained, counterstained with uranyl acetate and lead citrate, and examined with an Energy Filter Transmission Electron Microscope (EFTEM, ZEISS LIBRA® 120) equipped with a YAG scintillator slow scan CCD camera.

Golgi stain and dendritic spine density determination

One-month-old male mice were perfused transcardially with 0.9% NaCl in distilled water. Brains were taken and immersed in Golgi-Cox solution of FD Rapid Golgi Stain Kit (Cat. PK 401, FD Neuro Technologies, Columbia, MD) for 1 week, in the dark, at room temperature. After the period of impregnation, brains were immersed in solution C (Cat. PK 401, FD Neuro Technologies, Columbia, MD) and processed according manufacturer's instructions. The brains were sliced, using a vibratome, at 100 μm thickness; during the operation, the sample was kept wet with solution C (Cat. PK 401, FD Neuro Technologies, Columbia, MD). Then slices were put on gelatinized slides (2% gelatin (Merk), 1% $KCr(SO_4)_2 \cdot 12H_2O$ (Carlo Erba) and stained in the dark. After washing twice (4 min) with double distilled water, slices were stained in staining solution (10 min), prepared according manufacturer's instructions. After three double distilled water washes, slides were dehydrated for 4 min in increasing percentages of ethanol (50, 75, and 95%; all Sigma-Aldrich) and washed four times (4 min) in 100% ethanol. Finally, slides were immersed three times (4 min) in xylene and mounted on coverslips with Entellam (Electron Microscopy Sciences). Images were taken with a 63x objective in a white field. Neurons were analyzed with Neuron Studio software and statistical analysis was done in GraphPad Prism v.7.

Electro-encephalographic (EEG) recording

ACN-Ctr and ACN-KO mice were anesthetized with isofluorane (5% (v /v) in 1 L/min O_2. Four screw electrodes (Bilaney Consultants GMBH, Dusseldorf, Germany) were inserted bilaterally through the skull over the cortex (anteroposterior, +2.0–3.0 mm; left–right 2.0 mm from bregma); a further electrode was placed into the nasal bone as ground. The 5 electrodes were connected to a pedestal (Bilaney, Dusseldorf, Germany) and fixed with acrylic cement (Palavit, New Galetti and Rossi, Milan, Italy). The animals were allowed to recover for a week from surgery before the experiment.

EEG activity was recorded in a Faraday chamber using a Power-Lab digital acquisition system (AD Instruments, Bella Vista, Australia; sampling rate 100 Hz, resolution 0.2 Hz) in freely moving awake mice. Basal cerebral activity was recorded continuously for 24 h (from 5 pm to 4 pm). Segments with movement artefacts or electrical noise were excluded from statistical analysis. All EEG traces were also analysed and scored for the presence of spikes, which were discriminated offline with the spike histogram extension of the software (LabChart v8 Pro Windows). Spikes were defined as having a duration < 200 ms with baseline amplitude set to 4.5 times the standard deviation of the EEG signal (determined during inter-spike activity periods, whereas repetitive spiking activity was defined as 3 or more spikes lasting < 5 s)

Statistical analysis

Statistical analysis was performed using GraphPad Prism software v7. For comparison of two samples, a two-tailed unpaired Students's t-test was used. If not otherwise stated, for multiple comparisons, ANOVA was used followed by Tukey's post-hoc test. Differences were considered significant when $p < 0.05$.

RESULTS

Deletion of Astro-CaN deranges protein expression at posttranscriptional level

To investigate the effect of the deletion of CaN from astrocytes on gene and protein expression in the CNS, we performed Next Generation RNA sequencing (RNA-Seq) and shotgun mass spectrometry proteomics (SG-MS) analyses of hippocampus and cerebellum of one month-old ACN-KO and ACN-Ctr mice. RNA-Seq did not reveal significant alterations in gene expression in whole tissue hippocampal and cerebellar preparations from ACN-KO compared with ACN-Ctr mice (SI Appendix Fig. S1). SG-MS proteomics (Fig. 1A) identified 1661 and 1456 proteins in whole-tissue hippocampal (Wht-Hip) and cerebellar (Wht-Cb) preparations, respectively. In hippocampal (Syn-Hip) and cerebellar (Syn-Cb) synaptosomal fractions 525 and 471 proteins, respectively, were identified (SI Appendix, Table S1). Quantification and identification of differentially expressed proteins (DEPs) (FC > 50%, p-value < 0.05) yielded 21, 17, 134 and 40 DEPs in Wht-Hip, Wht-Cb, Syn-Hip and Syn-Cb samples, respectively (Fig. 1B and SI Appendix, Table S2). Surprisingly, there was very little, if any, overlap of DEPs between samples suggesting that the changes in protein expression produced by the deletion of Astro-CaN are brain region-specific. Validation of SG-MS results by WB (Fig. 1C) showed significant correlation ($R^2 = 0.612$, $p = 0.0044$) between SG-MS and WB (Fig. 1D). qPCR validation showed no alterations in mRNA levels except Vapa and Rab31, found to be downregulated in hippocampus confirming, thus, RNA-Seq results (SI Appendix Fig. S2). Classification of DEPs for Cell component and Function categories revealed that in Wht-Hip and Wht-Cb Cell components of *cytosol* were the most abundant followed by *mitochondria*, *ribosome* and *vesicles*, while among Functions there were *metabolism*, *translation*, *OXPHOS* followed by *vesicle trafficking* and *transport across membrane*. In synaptosomal preparations Cell components were categorized as *cytosol*, *cytoskeleton*, *mitochondria*, *plasma membrane*, *vesicles* and *ribosome*; while among Functions were *signalling*, *metabolism*, *transport across membrane*, *structural proteins*, *OXPHOS*, *translation* and *vesicle trafficking* (SI Appendix, Fig. S3).

Deletion of Astro-CaN deranges protein expression in major brain cell types

The analysis of DEPs showed the presence of many neuronal proteins, e.g., Thy-1, Snap25, Synaptophysin and Tau suggesting that the deletion of CaN from astrocytes affects neuronal protein expression. Priming the Human Protein Atlas database (https://www.proteinatlas.org/) in which protein expression is comprehensively examined using ATLAS antibodies (Sigma) and the cell-specificity of expression in the hippocampal formation is scored in glial and neuronal cells (Fig. 2A), revealed that, in the hippocampus, the majority of DEPs were neuron-specific (32.9%) or enriched in neurons (24.5%), while glia-specific protein (6.5%) or proteins enriched in glia (2.6%) were less abundant. Furthermore, priming the brain cell-specific transcriptome database published by Dr. Ben Barres and colleagues (Zhang et al., 2014), revealed that DEPs specific for all principal brain cell types, including astrocytes (8 hits), neurons (19 hits), oligodendrocytes (7 hits), microglial cells (3 hits) and endothelial cells (2 hits) were differentially expressed ACN-KO brain (Fig. 2B), corroborating and extending the results obtained using HPA.

Previously, we reported no alterations in neurodevelopment and brain cytoarchitecture of ACN-KO mice (Tapella et al., 2020), while SG-MS analysis showed consistent deregulation in expression of proteins associated to synapses. It thus was important to investigate if ACN-KO might have ultrastructural alterations of synapse organization. However, transmission electron microscope

analysis revealed no alterations in the neuropil of CA1 hippocampal region including synapses and mitochondria (SI Appendix, Fig. S4A). Likewise, quantification of dendritic spines in the hippocampus revealed no differences in spine density ($p = 0.78$, $n = 12$ for ACN-Ctr, $n = 15$ for ACN-KO), confirming that, at 1 mo of age, the deletion of CaN from astrocytes does not alter structural and morphological neuronal and synaptic organization of the CNS (SI Appendix, Fig. S4B).

Taken together, RNA-Seq and SG-MS analyses showed that at one month of age the deletion of Astro-CaN does not change transcription neither in the hippocampus nor in the cerebellum, while protein expression was altered differentially in these two brain regions, in all principal brain cellular types.

Deletion of Astro-CaN produces proteome signature of neuropathology and seizures

Next, we investigated functional significance of protein expression alterations in ACN-KO mice. For this analysis, whole-tissue DEPs were pooled with synaptosomal DEPs resulting in two lists, related to the hippocampus (HIP) and the cerebellum (CB). Gene ontology analysis of HIP DEPs revealed overrepresentation of 175 GO terms (SI Appendix, Table S3A). The most significantly overrepresented hits from GO category Cellular Component (CC) were *myelin sheath* (44 DEPs), *extracellular exosome* (90 DEPs) and *mitochondrion* (46 DEPs), while KEGG pathways were *OXPHOS* (17 DEPs), *Alzheimer's* (AD, 13 DEPs), *Parkinson's* (PD, 15 DEPs) and *Huntington's disease* (HD, 15 DEPs). Interestingly, intersection of *AD*, *PD*, *HD* and *OXPHOS* lists resulted in 12 common DEPs, all of which were components of the oxidative phosphorylation (OXPHOS) mitochondrial pathway (SI Appendix, Fig. S5). DAVID analysis of CB list returned 43 significantly overrepresented GO terms among which were KEGG pathway *ribosome* (7 DEPs) and CC *extracellular exosome* (33 DEPs), *intermediate filament* (7), *intracellular ribonucleoprotein complex* (9), *ribosome* (7) and *mitochondrion* (15) (SI Appendix, Table S3B). Presence of intermediate filaments of the keratin family was somewhat surprising, however priming databases Genecards (https://www.genecards.org/) and PaxDB (https://pax-db.org/) revealed presence of keratins in different brain proteome datasets (SI Appendix, Table S4).

Ingenuity pathway analysis (IPA) of HIP dataset resulted in a list of at least 500 significantly overrepresented annotations. Top Canonical Pathways were *Synaptogenesis Signaling Pathway*, *Phagosome Maturation*, *Sirtuin Signaling Pathway*, and *Mitochondrial Dysfunction* (Table 1). Overrepresented Disease And Functions annotations contained developmental and hereditary neurological disorders as well as psychiatric and neurodegenerative disorders (full list of annotations provided in SI Appendix, Table S5). Note the presence of annotations related to seizures and epilepsy (Table 1) which contained 29 proteins listed in (SI Appendix, Table S6). Top Upstream Regulators in HIP were proteins *MAPT*, *PS1*, *APP* and *HTT* (Table 1, and SI Appendix, Table S7A). Mutations of MAPT (Tau), PS1 and APP are the major causes of familial AD (FAD), while mutation of HTT is a cause of Huntington's disease. Of 69 unique proteins in *MAPT*, *PS1*, *APP* lists, 47 were common (SI Appendix, Table S7B), falling in three clusters, generated using STRING unsupervised k-means clustering, (i) neuronal and synaptic, (ii) metabolic pathways, mitochondrial and OXPHOS, and (iii) cytoskeletal and adhesion proteins (Fig. 3, and SI Appendix, Table S7C). Top Canonical Pathways in CB list were *EIF2 Signaling*, *Glucocorticoid Receptor Signaling*, *Regulation of eIF4 and p70S6K Signaling*, *Sirtuin Signaling Pathway* and *Mitochondrial Dysfunction*. Top Upstream Regulators in

CB were *MAPT*, *MYC* and *RICTOR*, while Disease And Functions annotations included *Decay of mRNA*, *Synthesis of protein*, *Parkinson's disease* and *Progressive encephalopathy* (Table 1).

Altogether, GO and pathway analyses suggest that the deletion of Astro-CaN affects, among others, mitochondrial function, protein synthesis and mTOR signalling, showing significant association with neurological diseases, including AD and epilepsy.

ACN-KO proteome shows significant overlap with 5xFAD mouse AD model and with human pharmacoresistant epilepsy datasets

Given the emergence of AD and seizures, we compared all our HIP ACN-KO DEPs with published AD and epilepsy proteome datasets. For AD comparison, we have chosen a proteome dataset obtained on 8 months-old 5xFAD mouse AD model, which represents the early stage of AD-like pathology (Neuner et al., 2017). HIP ACN-KO dataset showed significant overlap with 5xFAD-vs-NonTg proteome reported by Neuner et al. (18 overlapped proteins, p = 7.02E-15; Fig. 4A, and SI Appendix, Table S8A).

For comparison with epileptic brains, a dataset contributed recently by Karen-Aviram and colleagues (Keren-Aviram et al., 2018) has been chosen. This dataset features DEPs from the resected high frequency epileptic foci compared with biopsies of non-epileptic regions from the same patients with drug-resistant epilepsy (denominated as HE). Of 155 DEPs of HIP ACN-KO list, 26 DEPs (16.8%) were common with HE showing significant overlap (p = 1.07E-24; Fig. 4B, SI Appendix Table S8B).

Collectively, our omics data suggest that the deletion of CaN from astrocytes, at 1 mo of age produces deregulation of protein expression resembling that of AD and epilepsy.

ACN-KO mice develop tonic-clonic seizures and neuroinflammation starting from 5 months of age

The emergence of annotations related to seizures prompted us to investigate if these may be increased incidence of seizures during life-time of ACN-KO mice. Monitoring of ACN-KO mice revealed that starting from about 5 months of age, both males and females of ACN-KO mice showed increasing risk to develop seizures. Seizures started either upon cage opening, or upon bothering of a mouse by slight pulling the tail. The intensity of seizures corresponded to stages from 3 (forelimb clonus) to 5 (rearing and falling with forelimb clonus) according to Racine scale (Racine, 1972) or to stages 6-7 according to Pinel and Rovner scale (forelimb clonus with multiple rearing and falling; jumping) (Pinel and Rovner, 1978). The percentage of mice developing seizures grew steadily until 10 months after which the incidence did not increase (Fig. 5A). There were no differences in the risk of seizure development between the three experimental groups, males (n = 50), non-breading females (n = 36) and breading females (n = 80) (long-rank Mantel-Cox test, $\chi^2 = 0.856$, df = 2, p = 0.6518) reaching 40% risk for males and 45% for females (Fig. 5A). We next attempted registration of EEG in ACN-KO males. However, none of mice developed seizure after implantation of electrodes (n = 4) which made it impossible to register EEG during seizures. We thus, proceeded with registration of seizure-free mice. In all cases registered from ACN-KO mice there was a presence of aberrant electrical activity (100.8 ± 19.25 spikes/24h in ACN-KO vs 3.5 ± 0.50 spikes/24h in ACN-Ctr, p = 0.042, n = 5) resembling that of interictal spikes (Lévesque et al., 2018) (Fig. 5B). Neuroinflammation is a key feature of human seizure disorder and mouse models of epilepsy (van Vliet et al., 2018). Therefore, we investigated if in ACN-KO mice with seizures this key feature of epileptic brain was respected.

qPCR experiments on mRNA extracted from hippocampi of ACN-Ctr (labelled as Ctr in Fig. 5C), ACN-KO mice without seizures (labelled as Ns in Fig. 5C) and ACN-KO mice with recurrent seizures (labelled as Seiz in Fig. 5C) demonstrate that Il-1β, TNF, Cox2 and Gfap mRNA were significantly upregulated in ACN-KO mice with seizures (15.6 fold, $p < 0.0001$; 3.9 fold, $p = 0.0003$; 7.62 fold, $p = 0.0001$ and 1.29 fold, $p = 0.0067$, compared with ACN-Ctr, respectively), indicating an ongoing neuroinflammatory process. Together, our data suggest that the deletion of CaN from astrocytes results in development of delayed spontaneous tonic-clonic seizures from 5 months of age.

DISCUSSION

The present study was designed to investigate the effect(s) of the deletion of Astro-CaN on global transcriptional and translational remodelling in the CNS of ACN-KO mice at 1 month, a time-point when the CaN KO is fully expressed, development and neuronal differentiation in the CNS are completed, while there are minimal compensatory effects of the deletion of Astro-CaN. The principal findings of this work are: (i) in resting conditions, Astro-CaN does not have significant transcriptional activity; (ii) at 1 month of age, protein expression was altered in both hippocampus and cerebellum of ACN-KO mice in a brain area-specific manner, yet the expression of a distinct sets of proteins have been altered in hippocampal and cerebellar synaptosomes; (iii) changes in protein expression occurred in all principal cellular types of the CNS including astrocytes, neurons, oligodendrocytes, microglia and endothelial cells; (iv) bioinformatic analysis revealed overrepresentation of differentially expressed proteins related to neurodegenerative diseases, specifically to AD and seizure disorder; (v) comparisons with published proteome datasets indicate significant overlap of HIP ACN-KO dataset with those related to AD and epilepsy; and (vi) beginning from about 5 months of age ACN-KO mice show increased risk to develop tonic-clonic seizures.

Posttranscriptional nature of the Asro-CaN deletion effects

In astrocytes, CaN activity is mainly associated with transcriptional remodelling through activation of transcription factors NFAT and NF-kB. Such a transcriptional remodelling has been shown in several pathological conditions *in vivo* and *in vitro* in response to toxic or pro-inflammatory stimuli (Fernandez et al., 2012; Furman and Norris, 2014; Lim et al., 2016a). Neuronal activity-dependent activation of CaN as followed by NFAT nuclear translocation, has been demonstrated in pericytes after field stimulation of hippocampal slices (Filosa et al., 2007), while *in vitro* we have shown a robust Astro-CaN activation in mixed neuron-astrocytes hippocampal cultures upon chemical induction of long-term potentiation (LTP) (Lim et al., 2018). Here we show that the remodelling of CNS proteome, as a result of the deletion of CaN from astrocytes, occurs in the absence of transcriptional alterations, suggesting that the principal mean by which CaN acts in healthy astrocytes is through protein de-phosphorylation. However, it should be emphasized that for RNA-Seq and SG-MS analyses we used resting, not stimulated and not stressed animals. Therefore, at least in principle, a stress-or-stimulation-induced Astro-CaN-mediated transcriptional activity, as it occurs in neurons during late phase of LTP (Baumgärtel and Mansuy, 2012), cannot be *a priori* ruled-out. Nevertheless, we can speculate that, upon continuous change in homeostatic demand during dynamic neuronal activity, fast dephosphorylation/phosphorylation signalling would be more advantageous with respect to relatively slower transcription.

Astro-CaN deletion predicts neuropathology, does it mean that neuropathology is caused by Astro-CaN dysfunction?

The central finding of this work is that, in response to the deletion of CaN from astrocytes, the molecular signature of neuropathology was evident already at 1 month of ACN-KO mouse age. As shows gene ontology analysis, the molecular signature may be attributable to several neurological and neurodegenerative diseases, e.g., OXPHOS alterations were common between PD, HD and AD. However, IPA pathway analysis indicates on a particular link with AD. Strikingly, the top 3 Upstream Regulators found by IPA analysis were three major causes of FAD, namely Tau (MAPT), PS1 and APP with 47 common proteins downstream of these hypothetical regulators (30.3% of HIP list, SI Appendix Table 7B). Because of FAD mutated proteins have been traditionally regarded as neuronal proteins, one could draw a straightforward conclusion that the deletion of CaN from astrocytes predisposes neurons to harmful effects of FAD mutations creating partly fingerprint of FAD-related proteome. Analysis of cells-specificity of this list shows that the majority of proteins are, indeed, neuron-specific or enriched in neurons (Fig. 3B). This *in silico* analysis confirms the main thesis that is going to be suggested in this work: we propose a key role of Astro-CaN as a homeostatic regulator in the CNS and that the alterations in its activity predispose neurons to dysfunction.

Of special interest is the overlap with a mouse model of incipient AD, 8 months-old 5xFAD mice (Neuner et al., 2017). However, because of ACN-KO mice do not bear FAD mutations, it is unlikely that ACN-KO mouse represents an AD mouse model. Instead, significant overlap with hippocampal proteome of 5xFAD mice suggest that the alterations of Astro-CaN activity may occur during AD pathogenesis. Moreover, we propose that it may constitute a common denominator for a group of neuropathological diseases as suggested by bioinformatic analysis. In this light, considering the increased risk of seizures in AD patients (Nicastro et al., 2016; Vossel et al., 2017), the association of Astro-CaN KO specifically with AD and epilepsy assumes particular significance. Therefore, investigation of Astro-CaN activity and its association with central and peripheral markers at early disease stages may lead to the development of novel approaches in diagnosis, prevention and therapy of neuropathology.

Is ACN-KO mouse a novel model of spontaneous seizures and epilepsy?

Another important finding of this contribution regards the increased risk of ACN-KO mice to develop motor seizures in the period from 5 to 12 months of age. As we have previously reported, to 20th postnatal day ACN-KO mice develop full CaN KO in the hippocampus and the cerebellum (Tapella et al., 2020). Therefore, it is reasonable to suggest that the seizures are unlikely to be the direct effect of Astro-CaN KO. A delay of 5-10 month from the CaN-KO till seizure development suggests that a constellation of long-lasting alterations, downstream of Astro-CaN, may lead to seizure development. While the primary cause is represented by the Astro-CaN KO, the very cause of seizures is currently unknown. At the time of seizures ACN-KO mice show inflammatory phenotype closely resembling that observed in human disease and animal models of epilepsy (van Vliet et al., 2018). However, despite that the onset and development of epilepsy are strongly associated with neuroinflammation (Vezzani et al., 2019), it is prematurely to conclude that the seizures in ACN-KO mice are caused by the inflammatory process. Moreover, at 1 month of age of ACN-KO mice, the molecular epileptic fingerprint does not evidence inflammatory component but strongly suggests the insufficiency of glial support to neurons because: (i) primary cause is the deletion of an astroglial enzyme; (ii) altered expression of astrocyte-specific membrane transporters as Glast (Dematteis et al., 2020), Glt-1 and Atp1a2; and (iii) overrepresentation of DEPs related to myelin sheath suggesting inadequate oligodendrocytic function. In support of this, compromised myelinisation of axons in hippocampus

has been repeatedly associated with insurgence of seizure (Ye et al., 2013; Song et al., 2018). In this light, the significant overlap 1 mo-old ACN-KO mice proteome with that from human patients with intractable epilepsy (Keren-Aviram et al., 2018) is of special interest. Indeed, Keren-Aviram and colleagues reported downregulation of GFAP in the epileptic foci and did not report appearance of other makers of neuroinflammation.

Lastly, a "spontaneous" nature of seizures discriminates ACN-KO mice from the majority of animal models of epilepsy (Kandratavicius et al., 2014). We found that two third of ACN-KO mice do not develop seizures during their life-time, and the appearance of seizures cannot be predicted with absolute certainty. Manipulation with ACN-KO mice and/or surgical procedures decreases the probability to develop seizure to the extent that we were not able to register seizures in the electrode-implanted animals. All this renders ACN-KO mice time and cost-ineffective as a model of epilepsy (Kandratavicius et al., 2014). However, "fast" and cost-effective animal models are not able to faithfully reproduce all aspects of the human seizure disorder (Kandratavicius et al., 2014). This is particularly true for drug-resistant forms of epilepsy (Tang et al., 2017). We therefore, envisage that the results obtained from the thorough characterisation of epileptic phenotype of ACN-KO mice may outperform the time- and cost-related disadvantages of this novel and spontaneous model of seizure disorder.

Conclusion: Is Astro-CaN a master-regulator of homeostasis in the CNS?

The observations that glial cells change very early during neuropathology (Rodríguez et al., 2014; Verkhratsky et al., 2016) led to hypothesize that an insufficient homeostatic support to other cells in the CNS may be among the primary events which predispose neurons to dysfunction (Verkhratsky et al., 2016, 2019). In this context, we have proposed that deregulation of astroglial Ca^{2+} signalling, downstream of CaN, may contribute to this homeostatic failure (Lim et al., 2014, 2016b). Our present data provide further support to this hypothesis suggesting that Astro-CaN may work as a Ca^{2+}-sensitive hub orchestrating homeostatic activities of astrocytes. While molecular and signalling details of CaN activation and of Astro-CaN downstream signalling are a matter of future research, our results provide a framework for investigations suggesting that protein synthesis (Dematteis et al., 2020), myelination and mitochondria, alongside with mTOR signalling and with control of ion homeostasis (Tapella et al., 2020), may represent principal components of Astro-CaN-controlled homeostatic network.

AKNOWLEDGEMENTS

Funding: This work had the following financial supports: grants 2013-0795 to AAG, 2014-1094 to DL from the Fondazione Cariplo; grants FAR-2016 and FAR-2019 to DL from The Università del Piemonte Orientale; L.T. was supported by fellowship from the CRT Foundation (1393-2017).

Conflicts of Interest: The authors declare no conflict of interest.

REFERENCES

Baumgärtel K, Mansuy IM. 2012. Neural functions of calcineurin in synaptic plasticity and memory. Learn Mem 19:375–384.

Bindocci E, Savtchouk I, Liaudet N, Becker D, Carriero G, Volterra A. 2017. Three-dimensional Ca2+ imaging advances understanding of astrocyte biology. Science 356.

Dalla Pozza E, Manfredi M, Brandi J, Buzzi A, Conte E, Pacchiana R, Cecconi D, Marengo E, Donadelli M. 2018. Trichostatin A alters cytoskeleton and energy metabolism of pancreatic adenocarcinoma cells: An in depth proteomic study. J Cell Biochem 119:2696–2707.

Dematteis G, Restelli E, Chiesa R, Aronica E, Genazzani AA, Lim D, Tapella L. 2020. Calcineurin Controls Expression of EAAT1/GLAST in Mouse and Human Cultured Astrocytes through Dynamic Regulation of Protein Synthesis and Degradation. Available from: https://www.preprints.org/manuscript/202003.0234/v1

Dobin A, Davis CA, Schlesinger F, Drenkow J, Zaleski C, Jha S, Batut P, Chaisson M, Gingeras TR. 2013. STAR: ultrafast universal RNA-seq aligner. Bioinformatics 29:15–21.

Fernandez AM, Jimenez S, Mecha M, Dávila D, Guaza C, Vitorica J, Torres-Aleman I. 2012. Regulation of the phosphatase calcineurin by insulin-like growth factor I unveils a key role of astrocytes in Alzheimer's pathology. Mol Psychiatry 17:705–718.

Fiacco TA, Agulhon C, McCarthy KD. 2009. Sorting out astrocyte physiology from pharmacology. Annu Rev Pharmacol Toxicol 49:151–174.

Filosa JA, Nelson MT, Gonzalez Bosc LV. 2007. Activity-dependent NFATc3 nuclear accumulation in pericytes from cortical parenchymal microvessels. Am J Physiol, Cell Physiol 293:C1797-1805.

Furman JL, Norris CM. 2014. Calcineurin and glial signaling: neuroinflammation and beyond. J Neuroinflammation 11:158.

Gillardon F. 2006. Differential mitochondrial protein expression profiling in neurodegenerative diseases. Electrophoresis 27:2814–2818.

Gregorian C, Nakashima J, Le Belle J, Ohab J, Kim R, Liu A, Smith KB, Groszer M, Garcia AD, Sofroniew MV, Carmichael ST, Kornblum HI, Liu X, Wu H. 2009. Pten deletion in adult neural stem/progenitor cells enhances constitutive neurogenesis. J Neurosci 29:1874–1886.

Huang DW, Sherman BT, Lempicki RA. 2009. Systematic and integrative analysis of large gene lists using DAVID bioinformatics resources. Nat Protoc 4:44–57.

Kandratavicius L, Balista PA, Lopes-Aguiar C, Ruggiero RN, Umeoka EH, Garcia-Cairasco N, Bueno-Junior LS, Leite JP. 2014. Animal models of epilepsy: use and limitations. Neuropsychiatr Dis Treat 10:1693–1705.

Keren-Aviram G, Dachet F, Bagla S, Balan K, Loeb JA, Dratz EA. 2018. Proteomic analysis of human epileptic neocortex predicts vascular and glial changes in epileptic regions. PLoS ONE 13:e0195639.

Khakh BS, Sofroniew MV. 2015. Diversity of astrocyte functions and phenotypes in neural circuits. Nat Neurosci 18:942–952.

Lévesque M, Salami P, Shiri Z, Avoli M. 2018. Interictal oscillations and focal epileptic disorders. Eur J Neurosci 48:2915–2927.

Lim D, Mapelli L, Canonico PL, Moccia F, Genazzani AA. 2018. Neuronal Activity-Dependent Activation of Astroglial Calcineurin in Mouse Primary Hippocampal Cultures. Int J Mol Sci 19.

Lim D, Rocchio F, Lisa M, Fcancesco M. 2016a. From Pathology to Physiology of Calcineurin Signalling in Astrocytes | Opera Medica et Physiologica. Available from: http://operamedphys.org/OMP_2016_02_0029

Lim D, Rodríguez-Arellano JJ, Parpura V, Zorec R, Zeidán-Chuliá F, Genazzani AA, Verkhratsky A. 2016b. Calcium signalling toolkits in astrocytes and spatio-temporal progression of Alzheimer's disease. Curr Alzheimer Res 13:359–369.

Lim D, Ronco V, Grolla AA, Verkhratsky A, Genazzani AA. 2014. Glial calcium signalling in Alzheimer's disease. Rev Physiol Biochem Pharmacol 167:45–65.

Love MI, Huber W, Anders S. 2014. Moderated estimation of fold change and dispersion for RNA-seq data with DESeq2. Genome Biol 15:550.

Martinotti S, Patrone M, Manfredi M, Gosetti F, Pedrazzi M, Marengo E, Ranzato E. 2016. HMGB1 Osteo-Modulatory Action on Osteosarcoma SaOS-2 Cell Line: An Integrated Study From Biochemical and -Omics Approaches. J Cell Biochem 117:2559–2569.

Neilson JR, Winslow MM, Hur EM, Crabtree GR. 2004. Calcineurin B1 is essential for positive but not negative selection during thymocyte development. Immunity 20:255–266.

Neuner SM, Wilmott LA, Hoffmann BR, Mozhui K, Kaczorowski CC. 2017. Hippocampal proteomics defines pathways associated with memory decline and resilience in normal aging and Alzheimer's disease mouse models. Behav Brain Res 322:288–298.

Nicastro N, Assal F, Seeck M. 2016. From here to epilepsy: the risk of seizure in patients with Alzheimer's disease. Epileptic Disord 18:1–12.

Nikolic L, Nobili P, Shen W, Audinat E. 2019. Role of astrocyte purinergic signaling in epilepsy. Glia.

Oh-hora M, Rao A. 2008. Calcium signaling in lymphocytes. Curr Opin Immunol 20:250–258.

Parra V, Rothermel BA. 2017. Calcineurin signaling in the heart: The importance of time and place. J Mol Cell Cardiol 103:121–136.

Pinel JP, Rovner LI. 1978. Experimental epileptogenesis: kindling-induced epilepsy in rats. Exp Neurol 58:190–202.

Racine RJ. 1972. Modification of seizure activity by electrical stimulation. II. Motor seizure. Electroencephalogr Clin Neurophysiol 32:281–294.

Rocchio F, Tapella L, Manfredi M, Chisari M, Ronco F, Ruffinatti FA, Conte E, Canonico PL, Sortino MA, Grilli M, Marengo E, Genazzani AA, Lim D. 2019. Gene expression, proteome and calcium signaling alterations in immortalized hippocampal astrocytes from an Alzheimer's disease mouse model. Cell Death Dis 10:24.

Rodríguez JJ, Yeh C-Y, Terzieva S, Olabarria M, Kulijewicz-Nawrot M, Verkhratsky A. 2014. Complex and region-specific changes in astroglial markers in the aging brain. Neurobiol Aging 35:15–23.

Sitara D, Aliprantis AO. 2010. Transcriptional regulation of bone and joint remodeling by NFAT. Immunol Rev 233:286–300.

Song X-J, Han W, He R, Li T-Y, Xie L-L, Cheng L, Chen H-S, Jiang L. 2018. Alterations of Hippocampal Myelin Sheath and Axon Sprouting by Status Convulsion and Regulating Lingo-1 Expression with RNA Interference in Immature and Adult Rats. Neurochem Res 43:721–735.

Szklarczyk D, Morris JH, Cook H, Kuhn M, Wyder S, Simonovic M, Santos A, Doncheva NT, Roth A, Bork P, Jensen LJ, von Mering C. 2017. The STRING database in 2017: quality-controlled protein-protein association networks, made broadly accessible. Nucleic Acids Res 45:D362–D368.

Tang F, Hartz AMS, Bauer B. 2017. Drug-Resistant Epilepsy: Multiple Hypotheses, Few Answers. Front Neurol 8:301.

Tapella L, Soda T, Mapelli L, Bortolotto V, Bondi H, Ruffinatti FA, Dematteis G, Stevano A, Dionisi M, Ummarino S, Di Ruscio A, Distasi C, Grilli M, Genazzani AA, D'Angelo E, Moccia F, Lim D. 2020. Deletion of calcineurin from GFAP-expressing astrocytes impairs excitability of cerebellar and hippocampal neurons through astroglial Na+ /K+ ATPase. Glia 68:543–560.

Tu MK, Levin JB, Hamilton AM, Borodinsky LN. 2016. Calcium signaling in skeletal muscle development, maintenance and regeneration. Cell Calcium 59:91–97.

Verkhratsky A, Nedergaard M. 2018. Physiology of Astroglia. Physiol Rev 98:239–389.

Verkhratsky A, Parpura V, Vardjan N, Zorec R. 2019. Physiology of Astroglia. Adv Exp Med Biol 1175:45–91.

Verkhratsky A, Steardo L, Parpura V, Montana V. 2016. Translational potential of astrocytes in brain disorders. Prog Neurobiol 144:188–205.

Vezzani A, Balosso S, Ravizza T. 2019. Neuroinflammatory pathways as treatment targets and biomarkers in epilepsy. Nat Rev Neurol 15:459–472.

van Vliet EA, Aronica E, Vezzani A, Ravizza T. 2018. Review: Neuroinflammatory pathways as treatment targets and biomarker candidates in epilepsy: emerging evidence from preclinical and clinical studies. Neuropathol Appl Neurobiol 44:91–111.

Vossel KA, Tartaglia MC, Nygaard HB, Zeman AZ, Miller BL. 2017. Epileptic activity in Alzheimer's disease: causes and clinical relevance. Lancet Neurol 16:311–322.

Ye Y, Xiong J, Hu J, Kong M, Cheng L, Chen H, Li T, Jiang L. 2013. Altered hippocampal myelinated fiber integrity in a lithium-pilocarpine model of temporal lobe epilepsy: a histopathological and stereological investigation. Brain Res 1522:76–87.

Zhang Y, Chen K, Sloan SA, Bennett ML, Scholze AR, O'Keeffe S, Phatnani HP, Guarnieri P, Caneda C, Ruderisch N, Deng S, Liddelow SA, Zhang C, Daneman R, Maniatis T, Barres BA, Wu JQ. 2014. An RNA-sequencing transcriptome and splicing database of glia, neurons, and vascular cells of the cerebral cortex. J Neurosci 34:11929–11947.

HIPPOCAMPUS				CEREBELLUM		
Canonical Pathways	**p-value**	**# Hits**		**Canonical Pathways**	**p-value**	**# Hits**
Synaptogenesis Signaling Pathway	3.16E-15	21		EIF2 Signaling	9.77E-07	7
Phagosome Maturation	6.31E-15	16		Glucocorticoid Receptor Signaling	1.41E-04	6
Sirtuin Signaling Pathway	1.26E-12	18		Regulation of eIF4 and p70S6K Signaling	5.25E-04	4
Mitochondrial Dysfunction	1.26E-11	14		Sirtuin Signaling Pathway	6.31E-04	5
Remodeling of Epithelial Adherens Junctions	3.16E-11	10		Mitochondrial Dysfunction	7.24E-04	4
14-3-3-mediated Signaling	6.31E-11	12		Breast Cancer Regulation by Stathmin1	1.29E-03	4
Oxidative Phosphorylation	2.09E-10	11		mTOR Signaling	1.55E-03	4
Huntington's Disease Signaling	8.71E-10	14		Oxidative Phosphorylation	2.24E-03	3
Epithelial Adherens Junction Signaling	7.41E-09	11		Acetyl-CoA Biosynthesis III (from Citrate)	2.40E-03	1
Glycolysis I	1.82E-08	6		CCR3 Signaling in Eosinophils	3.24E-03	3
Upstream Regulator	**p-value**	**# Hits**		**Upstream Regulator**	**p-value**	**# Hits**
MAPT	1.97E-65	60		MAPT	1.89E-09	11
PSEN1	3.63E-49	50		MYC	6.71E-08	15
APP	4.24E-37	57		RICTOR	2.94E-07	8
HTT	4.63E-19	34		5-fluorouracil	1.50E-06	8
torin1	2.73E-16	15		MYCN	5.95E-06	7
metribolone	2.67E-15	24		HDAC4	2.03E-05	5
FMR1	6.96E-15	16		ammonia	3.56E-05	2
RICTOR	5.47E-14	19		LONP1	3.88E-05	4
sirolimus	9.3E-14	25		ST1926	4.87E-05	5
BDNF	1.28E-11	18		TLE3	5.46E-05	4
Diseases or Functions Annotation: Epilepsy	**p-value**	**# Hits**		**Diseases or Functions Annotation**	**p-value**	**# Hits**
Seizure disorder	4.07E-14	29		Decay of mRNA	1.30E-08	7
Seizures	4.47E-12	25		Synthesis of protein	2.35E-08	13
Infantile or early childhood epileptic encephalopathy	6.86E-12	12		Expression of protein	1.14E-07	11
Developmental epileptic encephalopathy	7.69E-12	12		Parkinson's disease	1.30E-07	9
Familial generalized epilepsy	4.56E-11	12		Nonsense-mediated mRNA decay	2.66E-07	6
Early-onset epilepsy	9.62E-11	13		Progressive encephalopathy	1.25E-06	14
Tonic-clonic seizure	2.68E-10	13		Movement Disorders	1.26E-06	16
Childhood epilepsy	9.85E-10	12		Progressive neuromuscular disease	1.26E-06	10
Epilepsy	1.34E-09	19		Initiation of translation of protein	1.48E-06	6
Epilepsy or neurodevelopmental disorder	4.79E-09	21		Disorder of basal ganglia	1.64E-06	13

Table 1. Top 10 overrepresented IPA annotations.

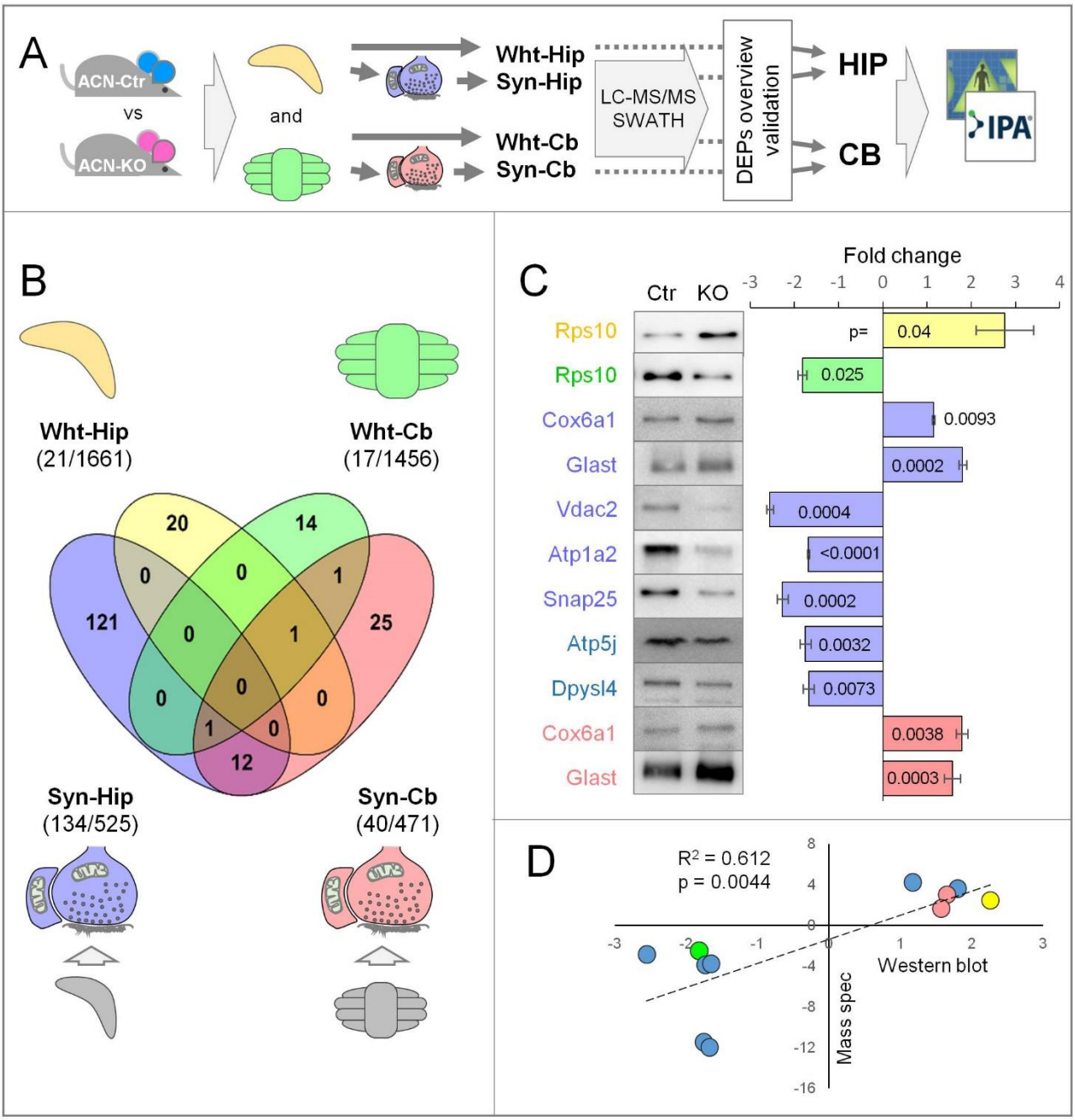

Fig. 1. Astrocyte-specific CaN knockout at 1 mo of age deranges protein expression differentially in the hippocampus and the cerebellum. (A) A scheme of the workflow: whole-tissue hippocampus (Wht-Hip) and cerebellum (Wht-Cb) and their respective synaptosomal fractions (Syn-Hip and Syn-Cb), prepared from ACN-Ctr and ACN-KO mice, were subjected either to NGS RNA sequencing (RNA-Seq, n = 6 mice per condition) or to shotgun mass spectrometry (SG-MS) proteomics (LC-MS/MS – SWATH, 4- 6 mice per condition). RNA-Seq did not result in a significant transcriptional activity. SG-MS resulted in 21, 17, 134 and 40 differentially expressed proteins (DEPs) in Wht-Hip, Wht-Cb, Syn-Hip and Syn-Cb, respectively. For bioinformatic analysis, hippocampal and cerebellar preparations were pooled resulting in HIP (155 DEPs) and CB (54 DEPs). (B) Intersection of DEPs lists show very limited overlap between samples indicating on brain region-specific alterations produced by Astro-CaN-KO. (C) Validation of DEPs by Western blot; and (D) correlation of Western blot results with SG-MS (R^2 = 0.612, p = 0.0044). Colour codes: cyan, ACN-

Ctr mice; magenta, ACN-KO mice; light-yellow, Wht-Hip samples, DEPs and proteins; light-green, Wht-Cb; light-blue, Syn-Hip; light-red, Syn-Cb.

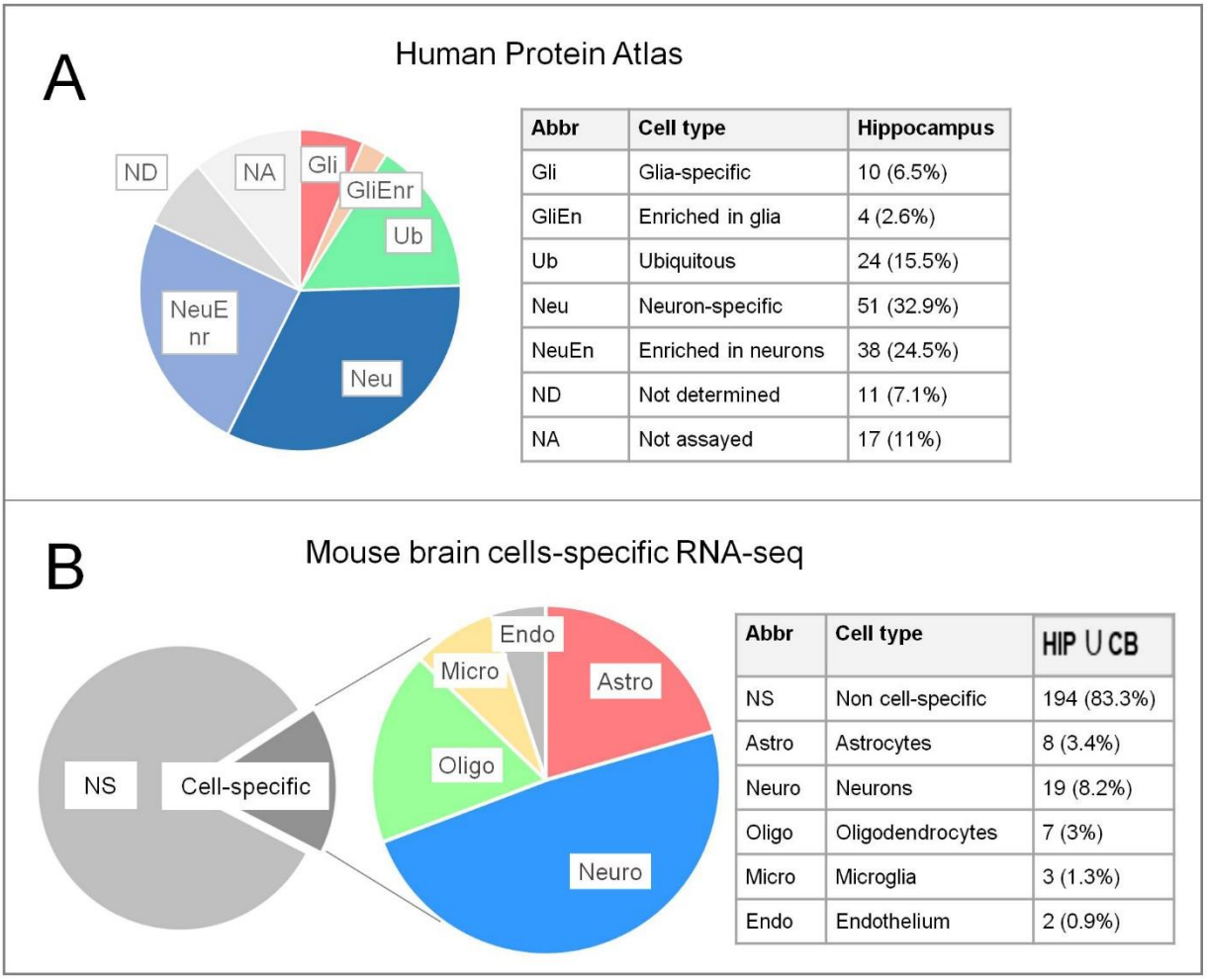

Abbr	Cell type	Hippocampus
Gli	Glia-specific	10 (6.5%)
GliEn	Enriched in glia	4 (2.6%)
Ub	Ubiquitous	24 (15.5%)
Neu	Neuron-specific	51 (32.9%)
NeuEn	Enriched in neurons	38 (24.5%)
ND	Not determined	11 (7.1%)
NA	Not assayed	17 (11%)

Abbr	Cell type	HIP ∪ CB
NS	Non cell-specific	194 (83.3%)
Astro	Astrocytes	8 (3.4%)
Neuro	Neurons	19 (8.2%)
Oligo	Oligodendrocytes	7 (3%)
Micro	Microglia	3 (1.3%)
Endo	Endothelium	2 (0.9%)

Fig. 2. Cell-specificity analysis of differentially expressed proteins. (A) Priming of Human Protein Atlas database (www.proteinatlas.org) of Hippocampal differentially expressed proteins (DEPs) revealed prevalence of neuronal DEPs. (B) Priming of mouse brain cell-specific RNA-Seq transcriptome revealed alterations in expression of proteins from all major CNS cell types, with prevalence of neuronal proteins.

A

UP-regulator	# Hits
MAPT	60
PSEN1	50
APP	57

Inersection

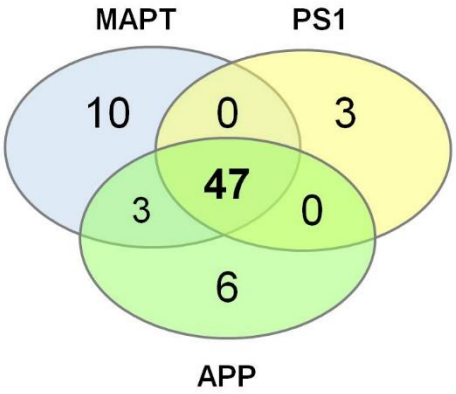

Cell-specificity

B

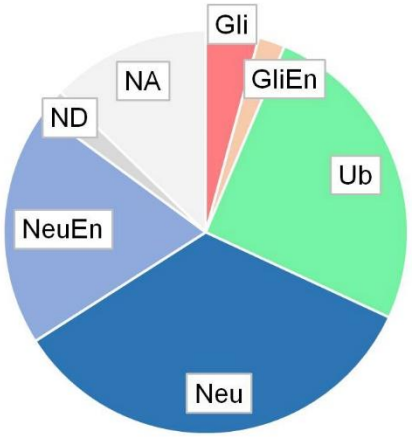

Abbr	Cell type	Hippocampus
Gli	Glia-specific	2 (4.3%)
GliEn	Enriched in glia	1 (2.1%)
Ub	Ubiquitous	12 (25.5%)
Neu	Neuron-specific	16 (34.0%)
NeuEn	Enriched in neurons	9 (19.1%)
ND	Not determined	1 (2.1%)
NA	Not assayed	6 (12.8%)

STRING k-means

C

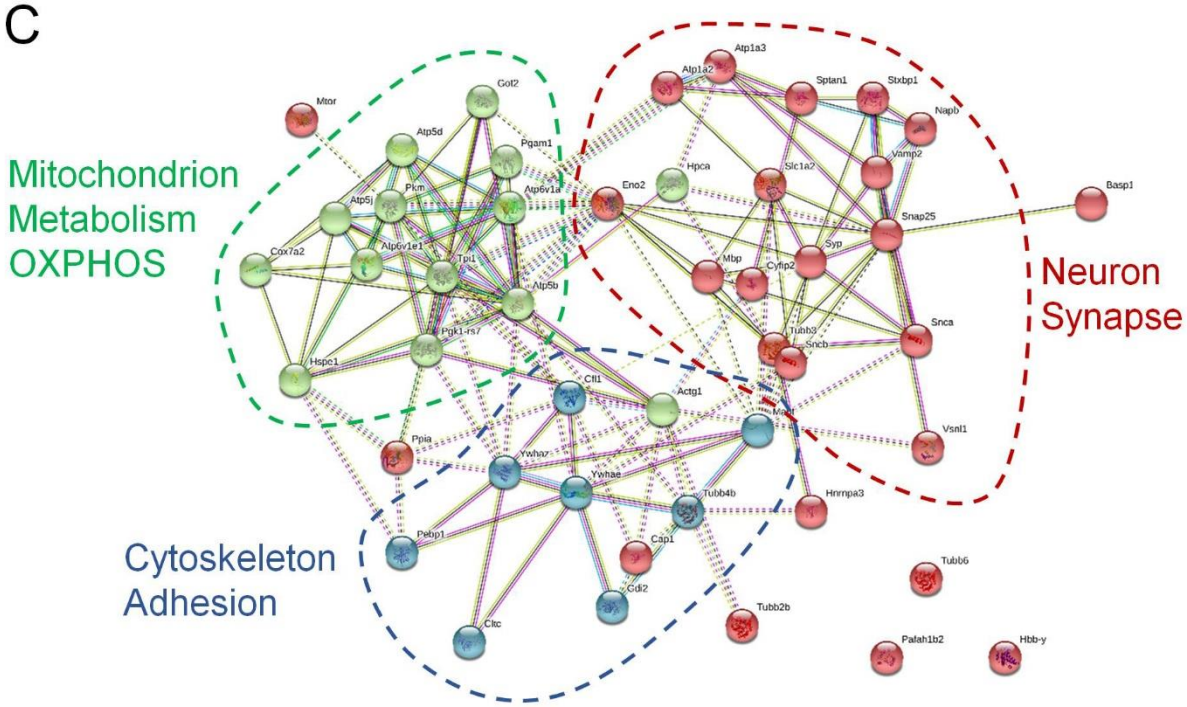

Fig. 3. Top 3 Cell-specificity and STRING k-means clustering of common targets of IPA pathway Upstream Regulators of Hippocampal DEPs MAPT, PS1 and APP. (A) Intersection of 60 MAPT, 50 PS1 and 57 APP putative regulated DEPs resulted in 47 common DEPs. (B) Cell-specificity analysis Huma Protein Atlas (www.proteinatlas.org) database shows presence of mostly neuronal and neuron-enriched DEPs. (C) 47 common DEPs regulated by MAPT, PS1 and APP, putative upstream regulators found by IPA pathway analysis, were subjected to STRING protein-protein interaction analysis. STRING k-means unsupervised clustering revealed 3 clusters grouped in proteins related to: neuron and synapse (Cluster 1, red), mitochondrion, metabolism and OXPHOS (Cluster 2, green); and cytoskeleton and adhesion (Cluster 3, light-blue).

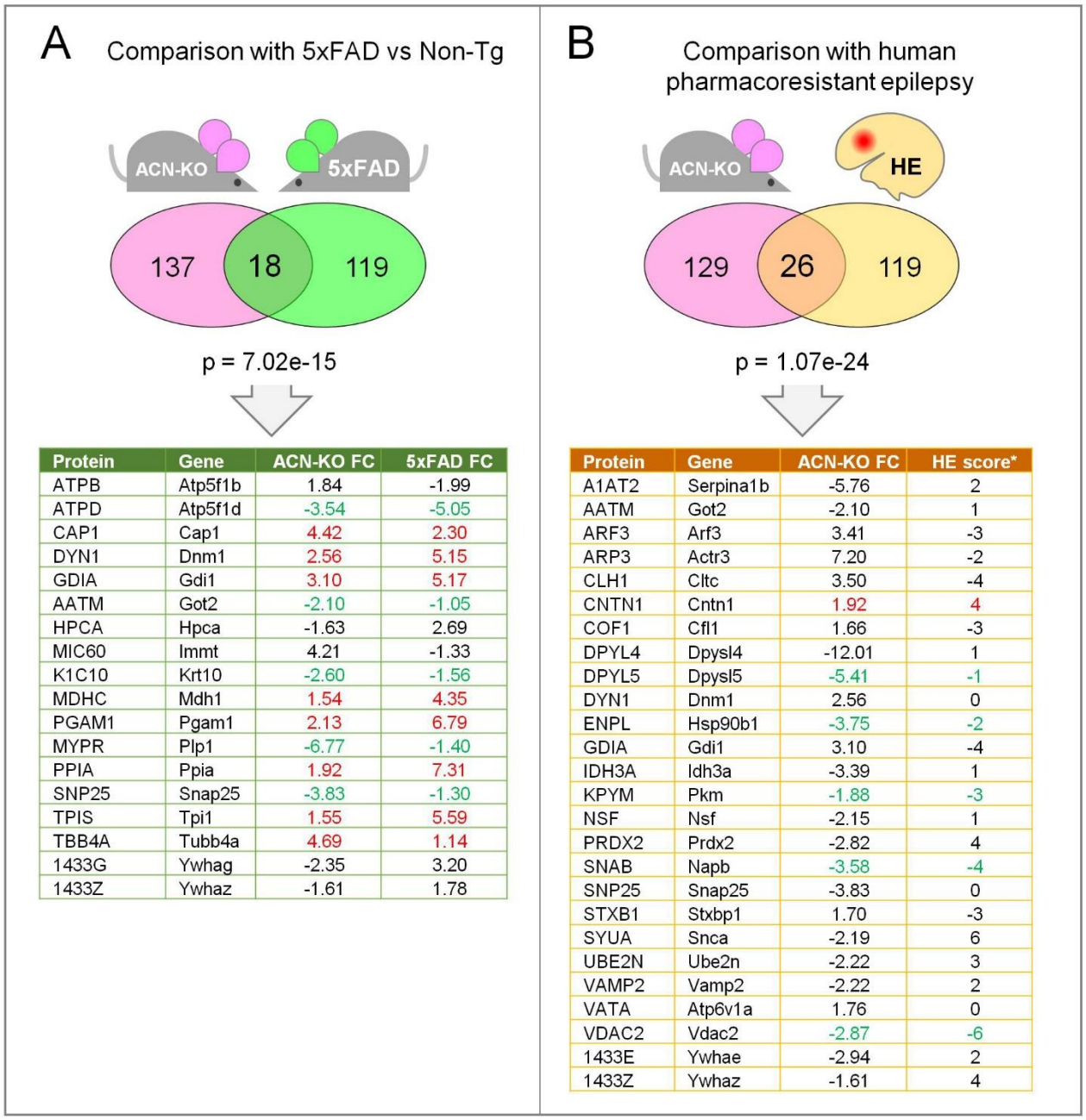

Protein	Gene	ACN-KO FC	5xFAD FC
ATPB	Atp5f1b	1.84	-1.99
ATPD	Atp5f1d	-3.54	-5.05
CAP1	Cap1	4.42	2.30
DYN1	Dnm1	2.56	5.15
GDIA	Gdi1	3.10	5.17
AATM	Got2	-2.10	-1.05
HPCA	Hpca	-1.63	2.69
MIC60	Immt	4.21	-1.33
K1C10	Krt10	-2.60	-1.56
MDHC	Mdh1	1.54	4.35
PGAM1	Pgam1	2.13	6.79
MYPR	Plp1	-6.77	-1.40
PPIA	Ppia	1.92	7.31
SNP25	Snap25	-3.83	-1.30
TPIS	Tpi1	1.55	5.59
TBB4A	Tubb4a	4.69	1.14
1433G	Ywhag	-2.35	3.20
1433Z	Ywhaz	-1.61	1.78

Protein	Gene	ACN-KO FC	HE score*
A1AT2	Serpina1b	-5.76	2
AATM	Got2	-2.10	1
ARF3	Arf3	3.41	-3
ARP3	Actr3	7.20	-2
CLH1	Cltc	3.50	-4
CNTN1	Cntn1	1.92	4
COF1	Cfl1	1.66	-3
DPYL4	Dpysl4	-12.01	1
DPYL5	Dpysl5	-5.41	-1
DYN1	Dnm1	2.56	0
ENPL	Hsp90b1	-3.75	-2
GDIA	Gdi1	3.10	-4
IDH3A	Idh3a	-3.39	1
KPYM	Pkm	-1.88	-3
NSF	Nsf	-2.15	1
PRDX2	Prdx2	-2.82	4
SNAB	Napb	-3.58	-4
SNP25	Snap25	-3.83	0
STXB1	Stxbp1	1.70	-3
SYUA	Snca	-2.19	6
UBE2N	Ube2n	-2.22	3
VAMP2	Vamp2	-2.22	2
VATA	Atp6v1a	1.76	0
VDAC2	Vdac2	-2.87	-6
1433E	Ywhae	-2.94	2
1433Z	Ywhaz	-1.61	4

Fig. 4 Comparison with 5xFAD mouse and human pharmacoresistant epilepsy proteome datasets. (A) Comparison with 8 mo old 5xFAD vs NonTg hippocampal proteome (18 common DEPs, listed in the table below; p = 7.02E-15) (Neuner et al., 2017). (B) Comparison with human drug-resistant epilepsy dataset contributed by (Keren-Aviram et al., 2018) obtained on brain biopsies from high-frequency epileptic foci vs low-frequency regions from the same patients. 26 common proteins were found (p = 1.07E-24) listed in the table below. Colour labels: in red co-upregulated; in green: co-downregulated DEPs.

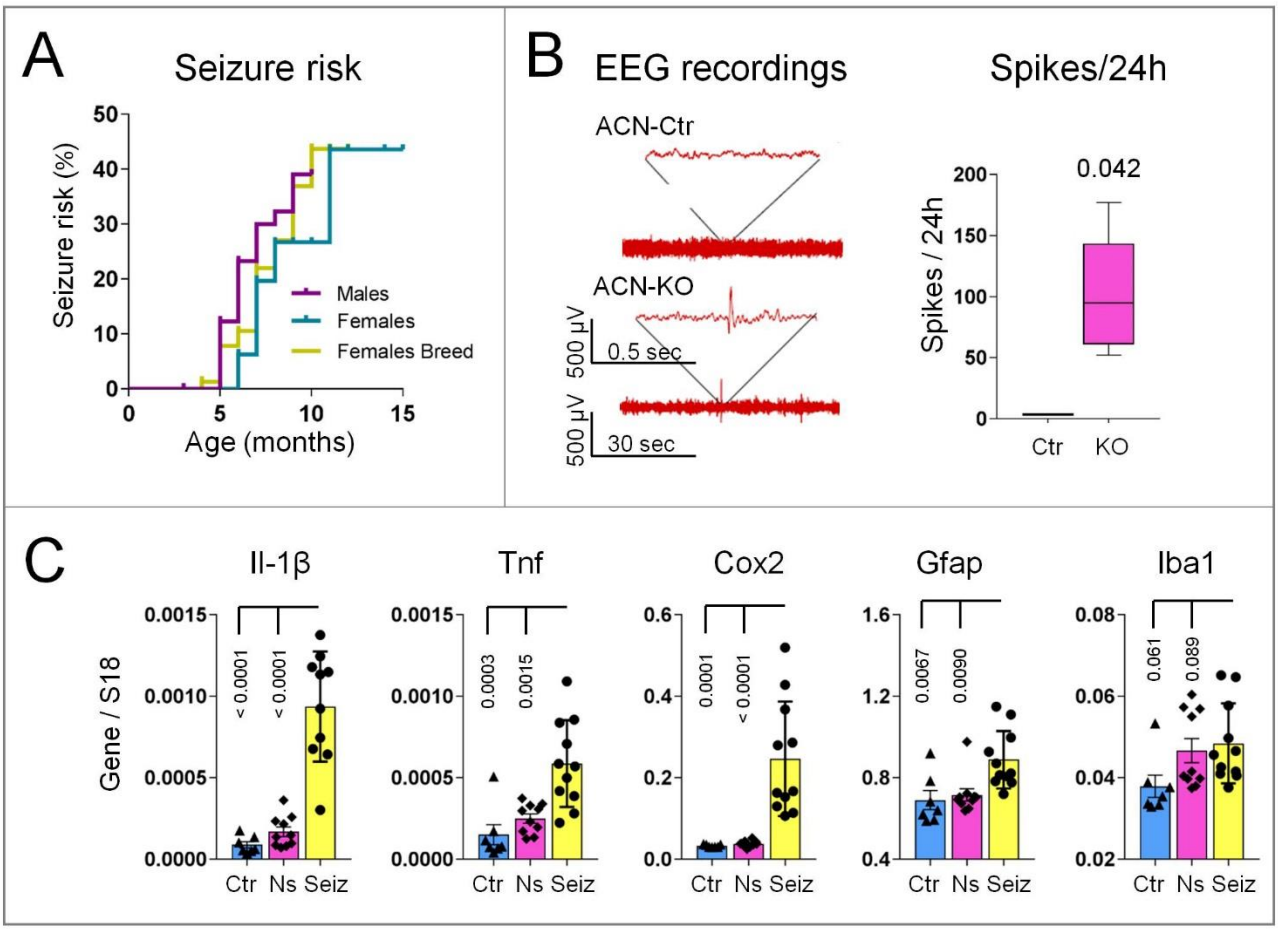

Fig 5. Increased risk to develop tonic-clonic seizures in ACN-KO mice beginning from 5 months of age, and inflammatory phenotype in 9 months-old ACN-KO mice with seizures. (A) Starting from 5 mo of age, both males and females exhibit increasing risk of spontaneous tonic-clonic seizures (violet, males, n = 50; turquoise, females, n = 36; yellow, females in breeding, n = 80, long-rank Mantel-Cox test, $\chi^2 = 0.856$, df = 2, p = 0.6518). (B) No seizures have been observed in mice which underwent surgery for electrode implantation. However, in seizure-free mice there were aberrant EEG spikes as registered by 24 h recording (100.8 ± 19.25 spikes/24h in ACN-KO vs 3.5 ± 0.50 spikes/24h in ACN-Ctr, p = 0.042, n = 5). (C) Hippocampi were dissected from ACN-Ctr (Ctr, cyan columns), ACN-KO mice which never had seizures (Ns, magenta columns) and from ACN-KO mice with seizures less than 5 min before sacrifice (Seiz, yellow columns). RNA was extracted and real-time PCR was performed using specific primers for pro-inflammatory cytokines (Il-1β, Tnf and Cox2) and markers of gliosis (Gfap and Iba1). Note upregulation of pro-inflammatory and gliotic markers specifically in ACN-KO mice with seizures ($p < 0.0001$, Seiz vs Ctr and Ns for Il-1β; p = 0.0003 and p = 0.0015, Seiz vs Ctr and Ns, respectively for Tnf; p = 0.0001 and $p < 0.0001$, Seiz vs Ctr and Ns, respectively for Cox2; p = 0.0067 and p = 0.0090, Seiz vs Ctr and Ns, respectively for Gfap; and p = 0.061 and p = 0.089, Seiz vs Ctr and Ns, respectively for Iba1).